J Therm Anal Calorim (2012) 110:593–599
DOI 10.1007/s10973-011-1948-0

Thermal and FTIR spectral studies of *N*,*N*′-diphenylguanidine

Q. Hu · H. L. Jin · X. A. Chen · S. Wang

Received: 22 July 2011 / Accepted: 21 September 2011 / Published online: 11 October 2011

Abstract Thermal decomposition of *N*,*N*′-diphenylguanidine (DPG) was investigated by simultaneous TG/DSC-FTIR techniques under nonisothermal conditions. Online FTIR measurements illustrate that aniline is a major product of DPG decomposition. The observation that the activation energy depends on the extent of conversion indicates that the DPG decomposition kinetics features multiple processes. The initial elimination of aniline from DPG involves two pathways because of the isomerization of DPG. Mass spectrometry and thin film chromatography suggest that there are two major intermediate products with the major one of $C_{21}N_3H_{17}$. The most probable kinetic model deduced through multivariate nonlinear regression method agrees well with the experimental data with a correlation coefficient of 0.9998. The temperature-independent function of conversion $f(\alpha)$, activation energy E and the pre-exponential factor A of DPG decomposition was also established through model-fitting method in this research.

Keywords Model-free methods · Nonisothermal decomposition kinetics · *N*,*N*′-diphenylguanidine (DPG) · TG/DSC-FTIR techniques · Mass spectrometry

Q. Hu · H. L. Jin · X. A. Chen · S. Wang (✉)
Nano-materials and Chemistry Key Laboratory,
Wenzhou University, Wenzhou, Zhejiang 325035, China
e-mail: shunwang@wzu.edu.cn

Q. Hu
Department of Pharmacology, School of Basic Medicine,
Hangzhou Normal University, Hangzhou, Zhejiang 310036,
China

Introduction

Guanidine and its derivatives have attracted a great deal of attention in materials science, biological and medicinal chemistry [1–18]. For example, guanidine derivatives have been widely used as vulcanization accelerators in rubber industry [1], insecticides in agriculture and antibacterial in medicine [2], hydrogen-bonding acceptor and donor in supermolecule formation [3–5], to name a few. In organic synthesis, guanidine derivatives have been widely used as excellent phase transfer catalysts in alkylation [6] and epoxidation [7] and as enantioselective base catalysts in asymmetric reactions [8, 9]. In biological systems, diverse benefits of guanidine derivatives, such as neuroleptic and antihypertensive activities [10, 11], the rescue of Arg mutations [12], the inhibitions of HIV-1 cell fusion [13] and poliovirus replication [14], have also been observed. In addition to the valuable applications mentioned above, various adverse effects, involving dermal irritation, necrosis and eschar formation and myelosuppression [15], have nevertheless been testified to interrelate with guanidine derivatives exposure.

Among substituted guanidines, 1,3-diphenylguanidine (DPG) has been used as a primary and secondary accelerator in the vulcanization of rubber and as both a collector and frother in selective flotation separation of mineral [16]. However, exposure to DPG may cause occupational allergic contact dermatitis [17], reproductive toxicology [18], cytostaticity and mutagenicity [19] during rubber manufacture or from contact with the finished products. Although it is well known that DPG could be broken down at high temperature, leading to the formation of carcinogenic aniline, little is known about the thermal decomposition kinetics of DPG. Kinetic studies of thermal decomposition of solids constitute one of the most

important applications of thermal analysis, in which the most common experimental technique is TG under the conditions of isothermal and/or nonisothermal conditions [20–24]. To shed light on thermal properties of the widely used DPG, herein we characterized the thermal stability of DPG under nonisothermal conditions by a simultaneous TG/DSC-FTIR method.

Experimental method

Preparation and characterization of DPG crystals

N,*N*′-diphenylguanidine (DPG) purchased from Zhejiang Ultrafine Powders & Chemicals Co., Ltd. (China) was recrystallized twice from chloroform, which resulted in the formation of colorless prisms. The DPG crystal structure was characterized by SMART APEX CCD single-crystal X-ray diffractometer (Bruker). Its crystal parameters (monoclinic, space group, $P2_1/c$) are identical to that observed by Tanatani et al. [25].

Thermal studies

Nonisothermal and simultaneous TG/DSC-FTIR measurements were performed with a Netzsch STA 409C thermoanalyser at heating rates of 278.15, 281.15, 283.15, 285.15 and 288.15 K min^{-1}. In a typical experiment, ~5.50 mg DPG crystals was heated from 283 to 773 K in an Al_2O_3 crucible under a dynamic nitrogen atmosphere at a flow rate of 100.0 mL min^{-1}. The gaseous thermal decomposition products were followed and analyzed by a Nicolet Avatar 470 FT-IR spectrometer. The solid products for the first thermal decomposition were produced by heating 2 g DPG in a railboat (95 mm × 12 mm × 12 mm) at 523 K for 1 h under nitrogen atmosphere at a flow rate of 100.0 mL min^{-1}. The as-obtained intermediates were dissolved in chloroform. The solvent was then evaporated under reduced pressure that resulted in the formation of yellowish-brown intermediate, which was further purified by TLC using precoated silica gel 60 F254 plates and flash column chromatography on Merck silica (300–400 mesh) using petroleum ether–ethyl acetate (3:1) as the eluent. Mass spectra of the major intermediate were obtained on a Thermo Finnigan DECAX-3000 LCQ Deca XP Plus after the sample was dissolved in acetonitrile. Elementary analysis was performed with EA-1112 (Italy).

Experimental observation of DPG thermal decomposition

Figure 1 presents the typical TG, DTG and DSC curves measured at a heating rate of 283.15 K min^{-1}. The TG

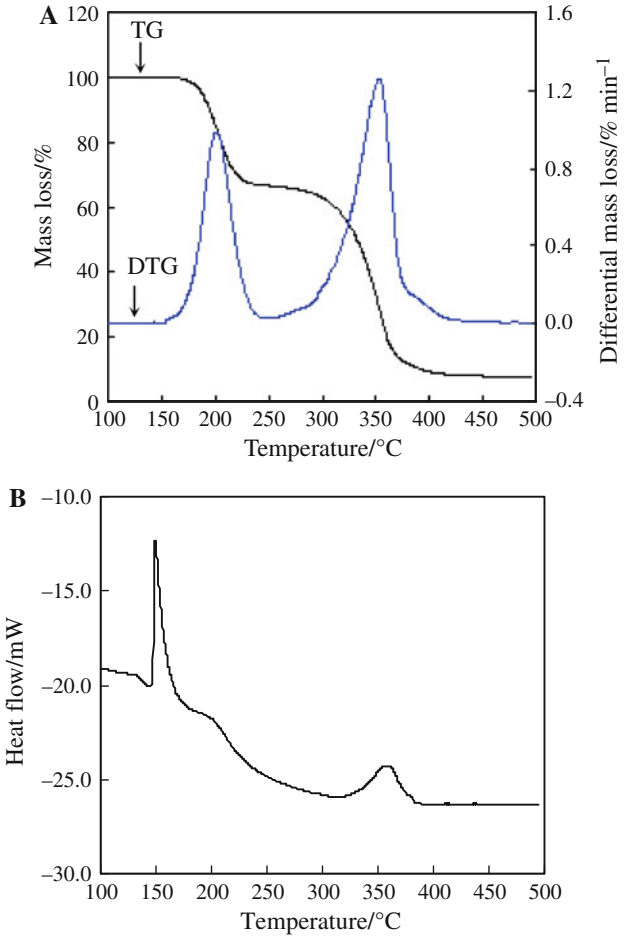

Fig. 1 TG/DTG/DSC curves of the thermal decomposition of DPG. The flow rate of nitrogen is 100 mL min^{-1}. The heating rate equals 10°C min^{-1} and the initial amount of DPG is 5.38 mg

curve in Fig. 1A, obtained over a temperature range of 283–773 K, illustrates that DPG decomposition goes through two stages. The first stage is between 435 and 528 K, whereas the second stage results in a further 63.62% mass loss between 528 and 773 K. This observation is consistent with the DTG curve that shows two peaks at 477.45 and 633.75 K, confirming the two stages of decomposition and the progressive mass loss observed in the TG curve as the temperature exceeds 435 K. The DSC curve in Fig. 1B displays three principal endothermic processes, in which the first endothermic process with the maximum of 423.15 K. As indicated by the TG curve, during the first endothermic process, there is nearly no mass loss, implicating that this process is dominated by the melting of DPG. Our experiments showed that the peak temperature of DPG fusion gradually increased with the heating rate β, in which a linear relationship was achieved. The second and third endothermic processes with the peak temperature of 478.05 and 639.05 K correspond to the two stages decomposition, respectively.

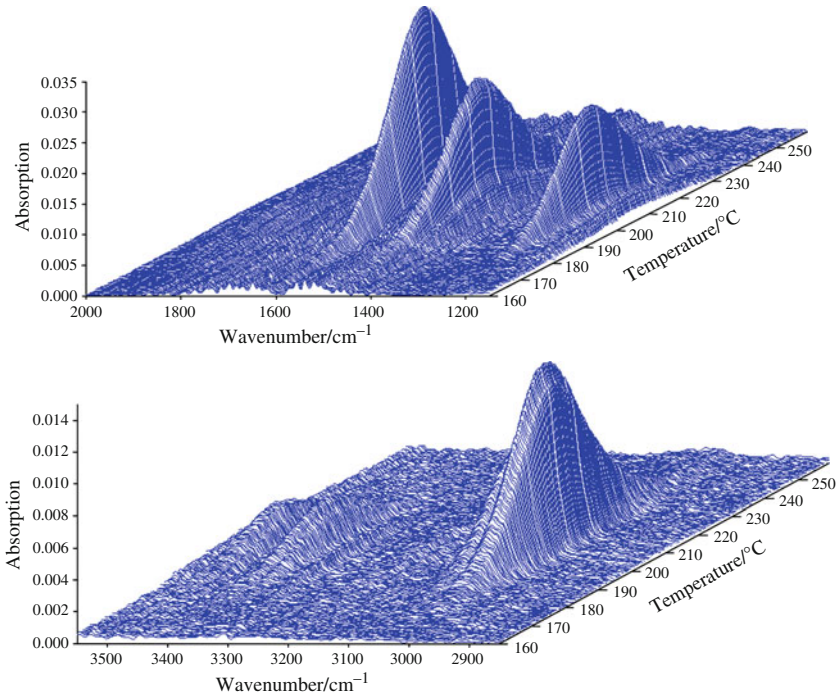

Fig. 2 Online FT-IR spectra of the off-gases of the pyrolysis of DPG. All reaction conditions are the same as those in Fig. 1

Figure 2 resulting in the escape of aniline that has characteristic absorption peaks at 3491, 3408, 3073, 3039, 1622, 1500, 1270, 1170 and 1083 cm^{-1} as shown in Fig. 2. Because the characteristic absorption peaks at 3491 and 3408 $cm^{-1}$of aniline are much smaller than those at 3073, 3039 1622, 1500, 1270, 1170 and 1083 cm^{-1}, Fig. 2 was shown as two parts with separate vertical scales. The second stage results in a further 63.62% mass loss between 528 and 773 K, which is probably a result of the subsequent pyrolysis of stable intermediates **I**. To decipher the nature of **I**, we have employed thin liquid chromatography method to separate **I** and identified two major products. After separation with flash column chromatography, mass spectroscopy was used to identify the products. The MS spectra have one major peak at *m/z* of 312, suggesting that the major composition of **I** is $C_{21}N_3H_{17}$. This result is further supported by elementary analysis (Theoretical C: 81.02%, N: 13.50%, H: 5.47%; experimental C: 80.73%, N: 13.61%, H: 5.65%). The second major component of **I** is an oligomer of aniline. This observation explains why the detected mass loss (ammonium and aniline gases) during the first stage is smaller than the theoretical value (i.e., because of the partial oligomorization of aniline).

Theoretical analysis of the decomposition kinetics

Model-free analysis

In nonisothermal TG study, model-fitting and model-free analysis are the two frequently used methods for the evaluation of kinetic parameters. The model-free method is based on isoconversional principle, especially the Friedman method [26], the Flynn–Wall–Ozawa method [27, 28] and Kissinger method [29] are of importance for kinetic analysis. Isoconversional kinetics rests on evaluating the dependence of the apparent activation energy on conversion or temperature and use such a dependence to make kinetic predictions or to derive the underlying reaction mechanism. These methods state that the reaction rate at a constant extent of conversion is only a function of the temperature [30]. Equation 1 is the differential form of Friedman and Eqs. 2 and 3 are the basic logarithm form of Flynn–Wall–Ozawa (FWO) and Kissinger.

$$\ln\left(\frac{\beta d\alpha}{dt}\right)_{\alpha} = \ln Af(\alpha) - \frac{E_{\alpha}}{RT_{\alpha}} \tag{1}$$

$$\ln(\beta) = \ln\left(\frac{AE_{\alpha}}{RG(\alpha)}\right) - 5.331 - 1.052\frac{E_{\alpha}}{RT_{\alpha}} \tag{2}$$

$$\ln\left(\frac{\beta}{T_{\mathrm{p}}^2}\right) = \ln\left(\frac{AR}{E}\right) - \frac{E}{RT_{\mathrm{p}}} \tag{3}$$

where R is the gas constant, A is the pre-exponential factor, E is the activation energy, β is the heating rate, α ($\alpha = \frac{\Delta W}{\Delta W_{\infty}}$) is the extent of conversion, T is the temperature, T_{p} is the peak temperature in the DSC curve and $f(\alpha)$ and $G(\alpha)$ are differential and integral model function, respectively. The activation energy related to a given conversion, E_{α}, can be obtained by plotting $\ln\left(\frac{\beta d\alpha}{dt}\right)_{\alpha}$ or $\ln(\beta)$ as a function of T_{α}^{-1} for various heating rates. The estimated values of the

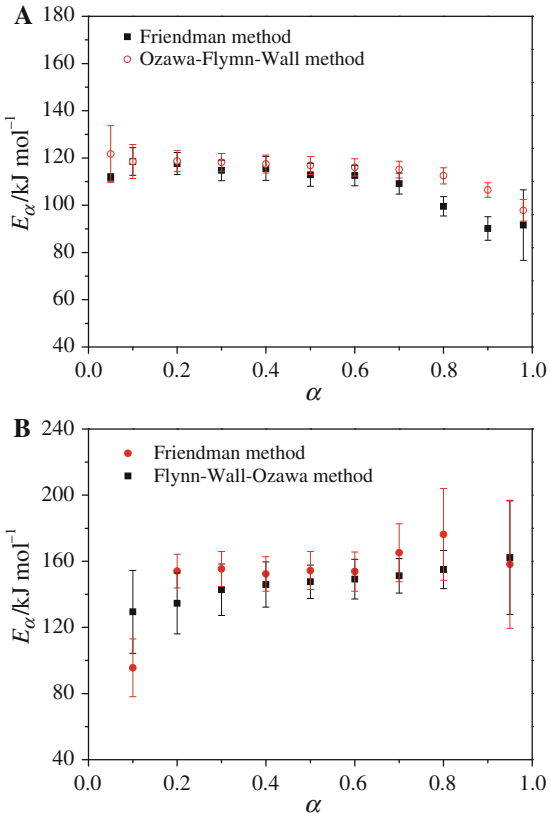

Fig. 3 Apparent activation energies (E_α) with *error bar* of **A** the first and **B** second stage of the thermal decomposition of DPG calculated with the Friedman method and the FWO method against the extent of conversion (α). The mass at $T = 528$ K and $T = 773$ K was used as the equilibrium mass for the first and second stage of the thermal decomposition of DPG, respectively

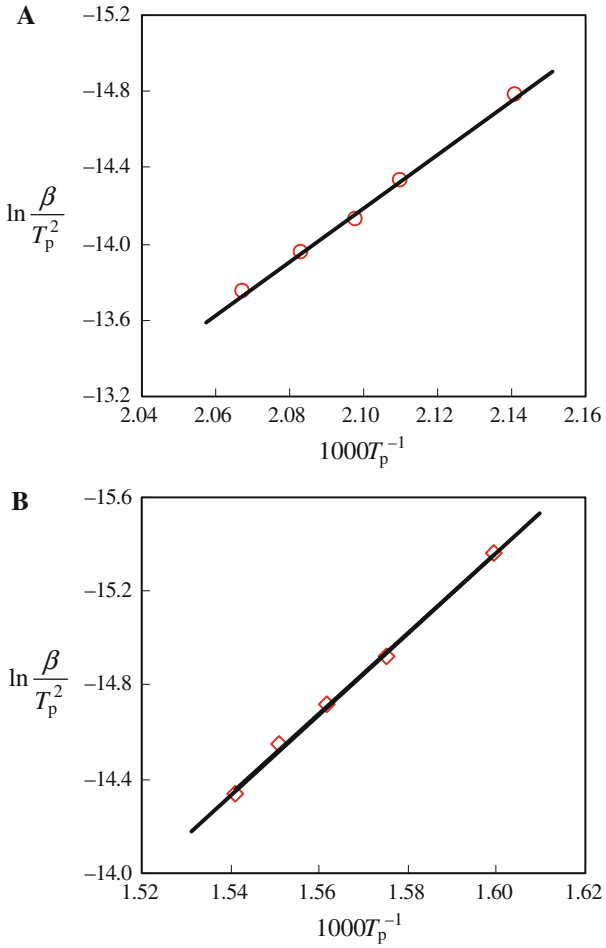

Fig. 4 The relationship between $\ln(\beta/(T_p)^2)$ and $1/T_p$ for the first (**A**) and second (**B**) thermal decomposition of DPG

apparent activation energy for the decomposition of DPG are presented in Fig. 3, which shows that the activation energy is dependent on the extent of conversion. Therefore, the two-stage decomposition kinetics of DPG is likely governed by multiple reaction steps [31]. As indicated by Fig. 3A, one can obtain the calculated activation energies (E) for DPG first-stage decomposition ranging from 90 to 120 kJ mol^{-1} (Friedman method) and 97 to 122 kJ mol^{-1} (Flynn–Wall–Ozawa method). Namely, the activation energy E equals 108.57 ± 5.37 kJ mol^{-1} (Friedman method) and 114.48 ± 4.84 kJ mol^{-1} (Flynn–Wall–Ozawa method) for the first- and second-stage decomposition of DPG, respectively. As shown in Fig. 3B, for the second-stage decomposition of DPG, the calculated activation energies equal 151.68 ± 17.33 (Friedman method) and 146.44 ± 16.81 kJ mol^{-1} (Flynn–Wall–Ozawa method). From the plots of $\ln(\beta/(T_p)^2)$ versus $(1/T_p)$ (Fig. 4), one obtains that the activation energy E equals 116.55 and 142.64 kJ mol^{-1} (Kissinger method) for the first and second-stage decomposition of DPG, respectively. These calculations illustrate that both methods agree with each other very well in estimating the activation energy of the thermal decomposition of DPG.

Model-fitting analysis

Model-fitting methods are among the first and most popular methods for kinetic description of thermal decomposition of solid. It requires only a single heating rate experiments to calculate the kinetic parameters. Several kinetic models are available in literature to describe the mechanism of solid-state reactions. The mechanism of the thermal decomposition reaction is usually found out by fitting the TG data into those kinetic models and choosing the one that gives the best fit. In this study, multivariate nonlinear regression from Netzsch Thermokinetics, which is based on multiple heating rates, was applied to carry out the fitting for DPG decomposition. Netzsch Thermokinetics is a comprehensive program for kinetic analysis of thermogravimetric (TG), differential scanning calorimetric (DSC), rheometric and dynamic mechanical analysis (DMA). Multivariate nonlinear regression, which is a key part of

Netzsch Thermokinetics, allows a direct fit of the model to experimental data without a transformation and has no limitations with respect to the complexity of the model. Earlier studies have demonstrated that the combination of model-free isoconversional methods and multivariate nonlinear regression can give more reasonable and applicable kinetics models than merely using model-fitting methods [32, 33].

DTG/DSC curves in Fig. 1 and the attained dependence of E on α suggest that there are at least three steps in the DPG thermal decomposition. At the initial stage, there is an exchange between the imino form R_1 and amino form R_2 of DPG, which is followed by the simultaneous decomposition from both forms. Working out from this hypothesis, a three-step reaction scheme

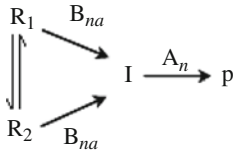

was proposed and tested with the 16 commonly used models [33]. To assure the derived kinetic equation is valid, values of E and A obtained through multivariate nonlinear regression method (model-fitting analysis) should agree with the numbers calculated with the model-free approach (e.g. Friedman and FWO methods). Therefore, models that yield with a high correction coefficient and a minimal Durbin–Watson [34] value shall represent the most probable kinetic model of the DPG decomposition. The corresponding function $f(\alpha)$ of Bna, expanded Prout-Tompkins equation (a-th degree autocatalytic reaction with an n-th order reaction) [35], is $(1-\alpha)^n\alpha^a$; $f(\alpha)$ of An (n-dimensional nucleation, Avrami–Erofeyev equation)

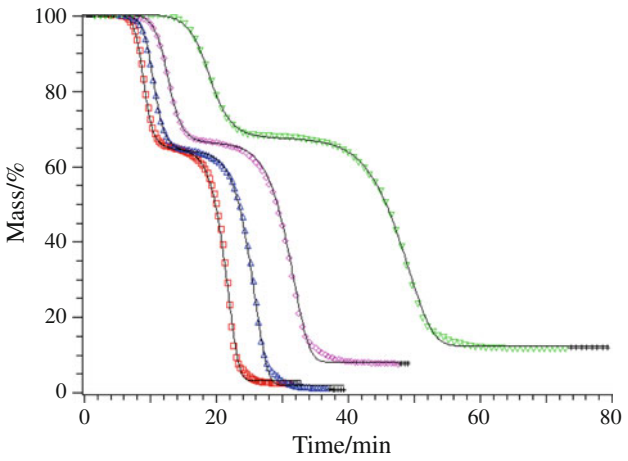

Fig. 5 Experimental and simulated TG curves of the thermal decomposition of DPG at heating rates of 5, 8, 10 and 12 °C min^{-1}. Symbols *open square*, *open up-pointing triangle*, *open diamond*, *open down-pointing triangle*: experimental curves; *line*: simulation curves

is $n(1-\alpha)[-\ln(1-\alpha)]^{1-\frac{1}{n}}$. Figure 3 shows that the calculated TG curves at heating rates of 5, 8, 10 and 12 °C min^{-1} are consistent with the experimentally measured data. The impressive fit between theoretical and experimental data is supported by the correlation coefficient, r, which is larger than 0.9998, and Durbin–Watson value (2.0147×10^{-3}). The fitted kinetic parameters are summarized in Table 1, which shows that the apparent activation energies calculated from the above-proposed models fall within the range derived from the variation of E as a function of α. Notably, the apparent activation energies of two parallel reactions (step 1 and step 2) are nearly equivalent, and their decomposition kinetics both follow expanded Prout–Tompkins equation, $f(\alpha)=(1-\alpha)^n\alpha^a$with

Table 1 Fitted kinetic parameters of DPG decomposition resulting from multivariate nonlinear regression (heating rates 5, 8, 10 and 12 °C min^{-1})

Reaction step	Model	n	a	E/kJ mol^{-1}	lg (A/s^{-1})	r	10^3DW
Step 1	B$_{na}$	2.1143	0.6676	122.35	10.40	0.9998	2.0147
Step 2	B$_{na}$	1.6585	0.5517	120.94	11.78		
Step 3	A$_n$	1.5035		160.14	10.77		

Bna the extended Prout–Tompkins equation $f(\alpha) = (1-\alpha)^n\alpha^a$, *An* the Avrami–Erofeyev equation $f(\alpha) = n(1-\alpha)[-\ln(1-\alpha)]^{1-\frac{1}{n}}$, r the correlation coefficient, *DW* the Durbin–Watson value

Fig. 6 The isomerization of *N*,*N*′-diphenylguanidine

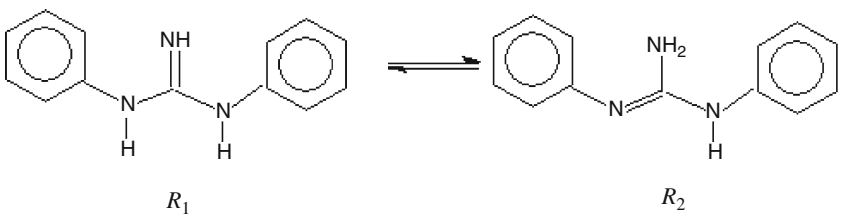

R_1 R_2

$n = 2.1143$, 1.6585 and $a = 0.6676$, 0.5517, respectively. The above results strongly suggest that the initial decomposition process consists of two parallel reactions that result from the isomerization of *N,N′*-diphenylguanidine (Fig. 5) (i.e., parallel decomposition of R_1 and R_2 of DPG). Such results lead us to believe that the decomposition of DPG follows the reaction model proposed in the preceeding (Fig. 6).

Conclusions

Thermal decomposition reaction of *N,N′*-diphenylguanidine (DPG) was investigated in this study by a simultaneous TG/DSC-FTIR method under nitrogen atmosphere. As evidenced by the thermoanalytical results, the DPG decomposition goes through two stages: The first stage is the loss of aniline from imino and amino forms of DPG, which is preceded by the tautomerization of DPG. Theoretical calculations show that the first-stage decomposition can be characterized by two expanded Prout–Tompkins equations and the corresponding rate laws can be represented as follows:

Step 1

$$\frac{d\alpha}{dt} = 2.5026 \times 10^{10} \times \exp\left(\frac{-122.35 \times 10^3}{RT}\right)(1-\alpha)^{2.1143}\alpha^{0.6676}$$

Step 2

$$\frac{d\alpha}{dt} = 6.08 \times 10^{11} \times \exp\left(\frac{-120.94 \times 10^3}{RT}\right)(1-\alpha)^{1.6583}\alpha^{0.5517}$$

The second stage is the subsequent pyrolysis of the stable intermediate **I**. Although we have not been able to determine the chemical structure of the substance **I**, the analysis nevertheless suggests that such an endothermic decomposition follows Avrami–Erofeyev equation, implicating that the second decomposition stage features random and continuous nucleation mechanism. Its rate law can be represented as follows:

Step 3

$$\frac{d\alpha}{dt} = 8.89 \times 10^{10} \times \exp\left(\frac{-160.14 \times 10^3}{RT}\right)(1-\alpha)[-\ln(1-\alpha)]^{0.3349}$$

In summary, the pyrolysis of DPG involves melting and subsequent two-stage decomposition that matches the reaction model proposed in the preceeding. The study on the decomposition of DPG shall be helpful to understand its thermal transformation process that is of significance for its applications.

Acknowledgements This work is supported through NSFC (21073133 and 20843007), Zhejiang Provincial Natural Science Foundation (Y4080177, Y4090248 and Y5100283) and Zhejiang Provincial Ministry of Education (Y200907715).

References

1. Sadequl AM, Ishiaku US, Poh BT. Cure index and activation energy of ENR 25 compared with SMR L in various vulcanization systems. Eur Polym J. 1999;35:711–9.
2. Kanne DB, Dick RA, Tomizawa M, Casida JE. Neonicotinoid nitroguanidine insecticide metabolites: synthesis and nicotinic receptor potency of guanidines, aminoguanidines, and their derivatives. Chem Res Toxicol. 2005;18:1479–84.
3. Otón F, Tárraga A, Molina P. A bis-guanidine-based multisignaling sensor molecule that displays redox-ratiometric behavior or fluorescence enhancement in the presence of anions and cations. Org Lett. 2006;8:2107–10.
4. Russell VA, Evans CC, Li WJ, Ward MD. Nanoporous molecular sandwiches: bonded networks with adjustable porosity. Science. 1997;276:575–9.
5. Schmidtchen FP, Berger M. Artificial organic host molecules for anions. Chem Rev. 1997;97:1609–46.
6. Kita T, Georgieva A, HashimotoY Nakata T, Nagasawa K. C_2-symmetric chiral pentacyclic guanidine: a phase-transfer catalyst for the asymmetric alkylation of tert-butyl glycinate Schiff base. Angew Chem Int Ed. 2002;41:2832–4.
7. Allingham MT, Howard-Jones A, Murphy PJ, Thomas DA, Caulkett PWR. Synthesis and applications of C_2-symmetric guanidine bases. Tetrahedron Lett. 2003;44:8677–80.
8. Terada M, Ube H, Yaguchi Y. Axially chiral guanidine as enantioselective base catalyst for 1,4-Addition reaction of 1,3-dicarbonyl compounds with conjugated nitroalkenes. J Am Chem Soc. 2006;128:1454–5.
9. Shen J, Nguyen TT, Goh YP, Ye W, Fu X, Xu J, Tan CH. Chiral bicyclic guanidine-catalyzed enantioselective reactions of anthrones. J Am Chem Soc. 2006;128:13692–3.
10. Olney JW, Labruyere J, Price MT. Pathological changes induced in cerebrocortical neurons by phencyclidine and related drugs. Science. 1989;244:1360–2.
11. Largent BL, Wikstrom H, Gundlach AL, Snyder SH. Structural determinants of sigma receptor affinity. Mol Pharmacol. 1987;32:772–84.
12. Guillén Schlippe YV, Hedstrom L. Guanidine derivatives rescue the Arg418Ala mutation of *Tritrichomonas foetus* IMP dehydrogenase. Biochemistry. 2005;44:16695–700.
13. Chang LC, Whittaker NF, Bewley CA. Crambescidin 826 and dehydrocrambine A: new polycyclic guanidine alkaloids from the marine sponge *Monanchora* sp. that inhibit HIV-1 fusion. J Nat Prod. 2003;66:1490–4.
14. Pfister T, Wimmer E. Characterization of the nucleoside triphosphatase activity of poliovirus protein 2C reveals a mechanism by which guanidine inhibits poliovirus replication. J Biol Chem. 1999;274:6992–7001.
15. Dubois SG, Messina J, Maris JM, Huberty J, Glidden DV, Veatch J, Charron M, Hawkins R, Matthay KK. Hematologic toxicity of high-dose iodine-131-metaiodobenzylguanidine therapy for advanced neuroblastoma. J Clin Oncol. 2004;22:2452–60.

16. Agnew R, Wilson SW, Stratton-Crawley R. Evaluation of flotation performance using variance spectrum analysis. Miner Eng. 1995;8:51–62.
17. Bruze M, Kestrup L. Occupational allergic contact dermatitis from diphenylguanidine in a gas mask. Contact Dermatitis. 1994; 31:125–6.
18. Bempong MA, Hall AV. Reproductive toxicology of 1,3-diphenylguanidine: analysis of induced sperm abnormalities in mice and hamsters and reproductive consequences in mice. J Toxicol Environ Health. 1983;11:869–78.
19. Bempong MA, Mantley R. Body fluid analysis of 1,3-diphenylguanidine for mutagenicity as detected by Salmonella strains. J Environ Pathol Toxicol Oncol. 1985;6:293–301.
20. Kotler JM, Hinman NW, Richardson CD, Scott JR. Thermal decomposition behavior of potassium and sodium jarosite synthesized in the presence of methylamine and alanine. J Therm Anal Calorim. 2010;102:23–9.
21. Bertol CD, Cruz AP, Stulzer HK, Murakami FS, Silva M. Thermal decomposition kinetics and compatibility studies of primaquine under isothermal and non-isothermal conditions. J Therm Anal Calorim. 2010;102:187–92.
22. Bayram H, Önal M, Hamza Y, Sarıkaya Y. Thermal analysis of a white calcium bentonite. J Therm Anal Calorim. 2010;101: 873–9.
23. Cabrales L, Abidi N. On the thermal degradation of cellulose in cotton fibers. J Therm Anal Calorim. 2010;102:485–91.
24. Burnham AK, Dinh LN. A comparison of isoconversional and model-fitting approaches to kinetic parameter estimation and application predictions. J Therm Anal Calorim. 2007;89:479–90.
25. Tanatani A, Yamaguchi K, Azumaya I, Fukutomi R, Shudo K, Kagechika H. N-methylated diphenylguanidines: conformations, propeller-type molecular chirality, and construction of water-soluble oligomers with multi-layered aromatic structures. J Am Chem Soc. 1998;120:6433–42.
26. Friedman HL. Kinetics of thermal degradation of char-forming plastics from thermogravimetry. Application to a phenolic plastic. J Polym Sci Part C. 1963;6:183–95.
27. Flynn JH, Wall LA. A quick, direct method for the determination of activation energy from thermogravimetric data. J Polym Sci Part B. 1966;4:323–8.
28. Ozawa T. A new method of analyzing thermogravimetric data. Bull Chem Soc Jpn. 1965;38:1881–6.
29. Kissinger HE. Reaction kinetics in differential thermal analysis. Anal Chem. 1957;29:1702–6.
30. Vyazovkin S. Modification of the integral isoconversional method to account for variation in the activation energy. J Comput Chem. 2001;22:178–83.
31. Vyazovkin S. A unified approach to kinetic processing of non-isothermal data. Int J Chem Kinet. 1996;28:95–101.
32. Opfermann J. Kinetic analysis using multivariate non-linear regression. J Therm Anal Calorim. 2000;60:641–58.
33. Zhang KL, Hong JH, Cao GH, Zhan D, Tao YT, Cong CJ. The kinetics of thermal dehydration of copper(II) acetate monohydrate in air. Thermochim Acta. 2005;437:145–9.
34. Durbin J, Watson GS. Testing for serial correlation in least squares regression I. Biometrika. 1950;37:409–28.
35. Brown ME, Dollimore D, Galwey AK. Reactions in the solid state. In: Bamford CH, Tipper CFH, editors. Comprehensive chemical kinetics. Elsevier, Amsterdam; 1980. p. 340.